



1 **Physical processes of cooling and megadrought in 4.2 ka BP event:**
2 **results from TraCE-21ka simulations**

3
4 Mi Yan^{1,2}, Jian Liu^{1,2*}, Liang Ning^{1,2,3}

5 ¹Key Laboratory of Virtual Geographic Environment, Ministry of Education; State
6 key Laboratory of Geographical Environment Evolution, Jiangsu Provincial
7 Cultivation Base; School of Geographical Science, Nanjing Normal University,
8 Nanjing, 210023, China

9 ²Jiangsu Center for Collaborative Innovation in Geographical Information Resource
10 Development and Application, Nanjing, 210023, China

11 ³Climate System Research Center, Department of Geosciences, University of
12 Massachusetts, Amherst, 01003, United States

13

14 *jliu@njnu.edu.cn

15

16

17



18

Abstract

19 It is widely believed that multidecadal to centennial cooling and drought occurred from
20 4500 BP to 3900 BP, known as the 4.2 ka BP event that triggered the collapse of many
21 cultures. However, whether this event was a global event or a regional event and what
22 caused this event remain unclear. In this study, we investigated the spatiotemporal
23 characteristics, the possible causes and the related physical processes of the event using
24 a set of long-term climate simulations, including one all-forcing experiment and four
25 single-forcing experiments. The results derived from the all-forcing experiment show
26 that this event occurred over most parts of the Northern Hemisphere (NH), indicating
27 that this event could have been a hemispheric event. The cooler NH and warmer
28 Southern Hemisphere (SH) illustrate that this event could be related to the slowdown
29 of the Atlantic Meridional Overturning Circulation (AMOC). The comparison between
30 the all-forcing experiment and the single-forcing experiments indicates that this event
31 was likely caused by internal variability. A positive North Atlantic Oscillation (NAO)-
32 like pattern in the atmosphere (low troposphere) triggered a negative Atlantic
33 Multidecadal Oscillation (AMO)-like pattern in the ocean, which then triggered a
34 Circumglobal Teleconnection (CGT)-like wave train pattern in the atmosphere (high
35 troposphere). The positive NAO-like pattern and the CGT-like pattern are the direct
36 physical processes that led to the NH cooling and megadrought. The AMO-like pattern
37 plays a “bridge” role in maintaining this barotropic structure in the atmosphere at a
38 multidecadal-centennial time scale. Our work provides a global image and dynamic
39 background to help better understand the 4.2 ka BP event.

40

41

42



43 **1 Introduction**

44 Understanding the characteristics and mechanisms of climate changes during the
45 Holocene can help predicting future changes, because there were warming periods in
46 Holocene induced by natural forcing comparable to current warming. The
47 multidecadal-to-centennial abrupt climate change, or the rapid climatic change during
48 ca. 4.5-3.9 ka BP (before 1950 CE), the so called “4.2 ka BP event”, was one of the
49 major climate events during the Holocene (Wang, 2009; Staubwasser and Weiss, 2006;
50 Mayewski et al., 2004; Wang, 2010). This event is considered to be closely linked to
51 the cultural evolutions of different regions of Eurasia such as the collapse of the
52 Akkadian empire, the termination of the urban Harappan civilization in the Indus valley
53 and the collapse of Neolithic Cultures around the Central Plain of China (Weiss et al.,
54 1993; Weiss and Bradley, 2001; Wu and Liu, 2001; Staubwasser et al., 2003; Wu and
55 Liu, 2004; An et al., 2005; Staubwasser and Weiss, 2006; Liu et al., 2013; Weiss, 2015,
56 2016). Moreover, this event is also thought to be the transition of the Middle to Late
57 Holocene (Walker et al., 2012; Finkenbinder et al., 2016) that inaugurated the “modern”
58 El Niño Southern Oscillation (ENSO) (Fisher et al., 2008). However, the characteristics,
59 causes and corresponding mechanisms behind this event remain unclear.

60 The 4.2 ka BP event is mostly characterized by rapid events at various latitudes
61 (Jansen et al., 2007), e.g., cooling in Europe (Lauritzen, 2003), centennial
62 megadroughts in North America (Booth et al., 2005), decreased precipitation in both
63 southern and northern China (Tan et al., 2008), and the weakened summer monsoon in
64 India (Nakamura et al., 2016); however, the manifestation of this event is far from
65 convincing and needs more evidence and simulation investigations (Roland et al., 2014).
66 Many reconstructions have shown that the 4.2 ka BP event is dominated by
67 megadroughts at centennial-scale over mid-low latitudes (Tan et al., 2008; Yang et al.,
68 2015; Weiss, 2016). However, Roland et al. (2014) found no compelling evidence, at
69 least in peatland records, to support that there was a 4.2 ka BP event in Great Britain
70 and Ireland. Moreover, according to the hydrologic cycle, it cannot be ruled out that
71 there were no flooding events somewhere else during this period. For example, Huang
72 et al. (2011) and Tan et al. (2018) found that successive floods occurred over the middle



73 reaches of the Yellow River in China in association with the abrupt climatic event of
74 4.2 ka BP.

75 Understanding the causes and mechanisms of the 4.2 ka BP event can provide
76 explanations for the reconstructed discrepancies over different regions. For the causes
77 of the event, some reconstruction studies have suggested that orbital forcing could have
78 played an important role in the early Holocene climate changes; however, no strong
79 evidence has shown that the solar forcing affected glacier fluctuations (cooling events)
80 in the late Holocene (Solomina et al., 2015). Tan et al. (2008) thought that the 4.2 ka
81 BP event could have been induced by the southward shift of the Intertropical
82 Convergence Zone (ITCZ) and oceanic sea surface temperature (SST) changes, as well
83 as the vegetation feedback caused by the solar activity. Liu et al. (2013) and Deininger
84 et al. (2017) argued that the atmospheric circulation, such as the North Atlantic
85 Oscillation (NAO)-like pattern but on a centennial time scale, could have played a more
86 important role than the ocean circulation in this event, although the mechanisms that
87 forced the circulation change remained unclear. A new reconstruction study has also
88 shown that the dry phases over the western Mediterranean in the period of 4.5 ka BP-
89 2.8 ka BP generally agreed with positive NAO conditions (Ramos-Román et al., 2018).
90 Additionally, there are discrepancies in the circulation pattern during the late Holocene
91 (Finkenbinder et al., 2016). Some studies show positive NAO-type patterns during the
92 late Holocene (Tremblay et al., 1997; Sachs, 2007; Ramos-Román et al., 2018), whereas
93 others show negative NAO-like patterns (Rimbu et al., 2004). Since the mechanisms
94 might could be a complex set of air-sea interactions (Roland et al., 2014), it is hard for
95 reconstruction to provide a general record due to its limitations such as interpretation
96 and spatially incompleteness. The mechanisms behind the 4.2 ka BP event need to be
97 clarified.

98 Therefore, to improve understanding of the 4.2 ka BP event, new high-resolution
99 reconstruction studies that focus on the 4.2 ka BP event are required. On the other hand,
100 physical-based modeling research can provide general concepts of the characteristics
101 of the event along with the causes and the mechanisms. Climate simulations have been
102 conducted to investigate another abrupt cooling event in the early Holocene, the so-



103 called 8.2 ka BP event. The simulations were used to test the hypothesis raised by the
104 reconstruction studies that the 8.2 ka BP event was most likely caused by freshwater
105 forcing and was associated with weakening of the Atlantic Meridional Overturning
106 Circulation (AMOC) (Morrill et al., 2013; Wagner et al., 2013; Morrill et al., 2014;
107 Matero et al., 2017; Ljung et al., 2008; Alley and Agustsdottir, 2005). For example, the
108 simulations argued that the meltwater from the collapse of the ice dome over Hudson
109 Bay was an essential forcing of the 8.2 ka BP event (Wagner et al., 2013; Matero et al.,
110 2017). However, little modeling work has been applied to the 4.2 ka BP event.

111 In the present study, we employed a set of transient climate simulation results to
112 investigate the characteristics of the 4.2 ka BP event and the possible causes and
113 mechanisms behind this event. The model and experiments are introduced in Sect. 2.
114 The results are shown in Sect. 3. The possible causes and mechanisms are discussed in
115 Sect. 4, and conclusions are drawn in Sect. 5.

116

117 **2 Model and experiments**

118 A set of transient simulations (TraCE-21ka, Simulation of Transient Climate
119 Evolution over the past 21,000 years, He, 2011) conducted with the Community
120 Climate System model version 3 (CCSM3) was used to investigate the spatial and
121 temporal characteristics of the 4.2 ka BP event and to determine the possible causes and
122 mechanisms behind this event. The experiments are listed in Table 1, including one
123 transient experiment with all-forcings (TraCE-ALL), one single-forcing experiment
124 forced only by transient orbital variation (TraCE-ORB), one single-forcing experiment
125 forced only by transient melt-water flux (TraCE-MWF), one single-forcing experiment
126 forced only by quasi-transient ice-sheet (TraCE-ICE), and one single-forcing
127 experiment forced only by transient greenhouse gases concentrations changes (TraCE-
128 GHG). The simulations were conducted from 22000 BP to 1990 CE for the TraCE-ALL,
129 the TraCE-ORB and the TraCE-GHG experiments, and from 19000 BP to 1990 CE for
130 the TraCE-MWF and the TraCE-ICE experiments.

131 The transient June insolation changes at 60°N and 60°S that resulted from the
132 orbital variation and the transient CO₂ change used in the simulations are shown in Fig.



133 1. The continental ice-sheet and topography changes are based on the ICE-5G (VM2)
134 reconstruction (He et al., 2013; Peltier, 2004). For the geography changes, the Barents
135 Sea opens at 13.1 ka BP, the Bering Strait opens at 12.9 ka BP, Hudson Bay opens at
136 7.6 ka BP, and the Indonesian Throughflow opens at 6.2 ka BP. The freshwater injected
137 into Northern Hemisphere (NH) and Southern Hemisphere (SH) oceans are based on
138 specific time slices (e.g., 19 ka BP into North Atlantic, 17 ka BP into North Atlantic,
139 11.5 ka BP into Arctic, St. Lawrence River, Hudson Strait, Barents Sea, North Sea, Ross
140 Sea and Weddell Sea). Note that no freshwater was delivered to the ocean after 5000
141 BP in the TraCE-ALL and TraCE-MWF experiments. The detailed information about
142 the experiments design can be referred to He (2011) and He et al. (2013).

143 The TraCE-21ka simulation was evaluated with reconstructions and was found
144 that it could reproduce major deglacial temperature evolutions (Clark et al., 2012;
145 Shakun et al., 2012). It has been used to depict the causes and mechanisms of Holocene
146 climate changes, such as the Bølling-Allerød warming (Liu et al., 2009), cooling into
147 the Younger Dryas and recovery to warm conditions (Liu et al., 2012) and the ENSO
148 evolution over the past 21 ka (Liu et al., 2014). In the present work, we adopted the
149 period of 5000 BP-3000 BP to focus on the 4.2 ka BP event.

150

151 **3 Results**

152 3.1 Identification of 4.2 ka BP event in the model simulation

153 The 101-year running mean annual NH surface temperature and precipitation
154 during 5 ka BP-3 ka BP shows double peak centennial cooling and drought from 4.4 ka
155 BP to 4.0 ka BP (Fig. 2, dashed black line). However, the variabilities are smaller over
156 the SH than those over the NH. There is no significant cooling and drought event during
157 that period (Fig. S1, dashed black line) over the SH. The SH precipitation even shows
158 a double-peak wet condition during the period of 4.4 ka BP-4.0 ka BP.

159 The double peak centennial cooling and drought are still obvious when the 31-year
160 running mean is applied to the time series (not shown), which indicates that the 4.2 ka
161 BP event has multidecadal to centennial variabilities. Moreover, the centennial
162 warming periods right before and after the 4.2 ka BP event indicate that this event might



163 be included in a quasi-millennium variation. Therefore, the 4.2 ka BP event could be a
164 multiscale event, i.e. from multi-decadal to millennium.

165 The seasonal mean NH surface temperature changes show that the annual mean
166 variability is dominated by the boreal winter (December-January-February, DJF)
167 surface temperature change (Figure S2). The correlation coefficient between the annual
168 mean NH surface temperature (NHT) and the DJF mean NHT is 0.96 (after the 101-
169 year running mean), which is significant above the 99% confidence level, much higher
170 than the correlation coefficient between the annual mean and the boreal summer (June-
171 July-August, JJA) mean of only 0.30 (after the 101-year running mean), which is not
172 significant. However, this is different for the precipitation change, for which both the
173 JJA mean and the DJF mean contribute to the annual mean precipitation change (not
174 shown).

175 To identify the characteristics of the 4.2 ka BP event, two centennial cool periods
176 and two centennial warm periods that exceeded ± 0.5 standard deviations are selected.
177 The two centennial cool periods span from 4320 BP to 4220 BP and from 4150 BP to
178 4050 BP, and the two centennial warm periods span from 4710 BP to 4610 BP and from
179 3980 BP to 3880 BP.

180

181 3.2 Spatial characteristics of surface temperature and precipitation

182 To help draw a coherent global view of the 4.2 ka BP event, the spatial
183 characteristics of temperature and precipitation changes during the 4.2 ka BP event are
184 shown in Fig. 3.

185 Figure 3a gives the spatial distribution of the annual mean surface temperature
186 difference between the cold periods and the warm periods. The cooling significantly
187 occurred over most regions of the NH, especially over the middle to high latitudes of
188 the NH and most land regions of the SH. Most parts of India, northern Mexico and the
189 middle latitudes of the SH ocean experienced warm conditions. Such asymmetric
190 change between the hemispheres (cool NH and warm SH) favors the southward shift of
191 the ITCZ. The spatial distribution of the surface temperature change is still dominated
192 by the boreal winter pattern (not shown). The large cooling over the NH and small



193 warming over the SH could be related to the orbital change, which induces insolation
194 increases over the SH but decreases over the NH.

195 The spatial distribution of annual mean precipitation differences between the cold
196 periods and the warm periods is shown in Fig. 3b. During the cold periods, significant
197 drought is mainly located over most regions of the NH, especially over Europe, western
198 Asia, and central and southern North America (or Intra America). For the SH, the land
199 precipitation increased, which indicates a southward shift of the ITCZ, as suggested by
200 the aforementioned asymmetric temperature change and by the previous studies based
201 on both reconstructions (Fleitmann et al., 2007; Cai et al., 2012) and simulations
202 (Broccoli et al., 2006). Over East China, the precipitation anomalies show a wet south-
203 dry north pattern, which indicates a weakened East Asian monsoon consistent with the
204 reconstruction record (Tan et al., 2018).

205 The sea surface temperature (SST) shows that the largest change occurs over the
206 northern Atlantic Ocean and then the northern Pacific Ocean (Fig. 4). The warmer south
207 and cooler north over the Atlantic Ocean indicates an Atlantic Multi-Decadal
208 Oscillation (AMO)-like pattern with its cold phase. The cold phase of the AMO has
209 been confirmed to induce summer rainfall decreases over India and Sahel in both
210 simulations and proxy data (Zhang and Delworth, 2006; Shanahan et al., 2009).

211 The simulated characteristics of the temperature change, the precipitation change,
212 and the SST change are similar to those responses to the weakened AMOC state (Brown
213 and Galbraith, 2016).

214

215 3.3 Circulations associate with the 4.2 ka BP event

216 The sea level pressure (SLP) differences between the cooler periods and the
217 warmer periods show that the largest change occurs over the mid-high latitudes of the
218 NH and SH (Figure 5a). The negative SLP anomalies over the high North Atlantic and
219 positive SLP anomalies over the middle North Atlantic during the cool periods resemble
220 a positive North Atlantic Oscillation (NAO)-like pattern but on a centennial-millennial
221 time scale. The positive NAO-like pattern is accompanied by cyclonic circulation over
222 Iceland and anticyclonic circulation over the Azores Islands and thus strengthened



223 westerlies over the downstream regions (Fig. 5a). The subtropical highs and the relative
224 anticyclones in both the SH and NH are strengthened during the cold periods from low
225 troposphere (850 hPa) to high troposphere (200 hPa), which illustrates a barotropic
226 structure (Fig. 5). The centers with positive geopotential height anomalies during the
227 4.2 ka BP event over Western Europe, Central Asia, East Asia, the east north Pacific
228 and Eastern North America, as well as the anti-cyclonic circulation anomalies at 200
229 hPa (Fig. 5d), resemble a Circumglobal Teleconnection (CGT)-like wave pattern (Ding
230 and Wang, 2005; Lin et al., 2016) but on a centennial-millennial time scale.

231 The strengthened subtropical highs with mid-latitudes anticyclones from lower to
232 upper levels are the direct physical processes that cause the precipitation decreases and
233 thus the following megadrought over mid-latitudes of NH regions, particularly over
234 Eurasia. The cooler land-warmer ocean over East Asia and the West Pacific (Fig. 3a)
235 indicate weakened land-ocean thermal contrast associated with higher SLP over land
236 and lower SLP over the adjacent ocean (Fig. 5a). The weakened land-ocean contrast
237 can lead to a weaker East Asian monsoon, accompanied by precipitation increases over
238 the southern China pattern and precipitation decreases over the northern China pattern
239 (Fig. 3b).

240

241 **4 Discussions**

242 The simulations show that the cool and dry conditions of the 4.2 ka BP event is
243 more like a hemispheric phenomenon, mainly located over the NH, rather than a global
244 phenomenon. The land over the SH experiences cool but wet conditions, and the mid-
245 latitude SH ocean is warmer. The potential causes and mechanisms of this event will be
246 discussed in this section.

247 **4.1 The possible causes of the 4.2 ka BP event**

248 Some records suggested that solar irradiance was one of the essential mechanisms
249 that drove the Holocene climate variation at centennial to millennial time scales (Bond
250 et al., 2001), whereas others suggested that the linkage between solar irradiance and
251 multicentury scale cooling events during the Holocene was weak, particularly in the
252 mid- to late-Holocene (Turney et al., 2005; Wanner et al., 2008). The solar irradiance is



253 not included in the experiments used in the present work. Nonetheless, we still obtain
254 multicentury cooling events (such as the 4.2 ka BP event) in the TraCE-ALL experiment.
255 This side-fact indicates that the solar irradiance might not be the driving factor for the
256 Holocene cooling events.

257 If the results derived from the TraCE-ALL experiment are consistent with those
258 derived from a particular single-forcing sensitivity experiment, we assume the variation
259 to be forced by that forcing. Otherwise, if the results derived from the TraCE-ALL
260 experiment differ from those from the single-forcing sensitivity experiments, we
261 assume the variation to be forced by the internal variability. In this section, we use the
262 series after applications of 101-year running means as an example and compare the
263 results derived from the all-forcing experiment to those derived from the single-forcing
264 experiment to determine the possible forcings that triggered the 4.2 ka BP event.

265 The correlation coefficients between the annual mean NHT derived from the
266 TraCE-ALL run and the NHT derived from each single-forcing run are listed in Table
267 2. There is no significant clue that the annual mean NHT variation is forced by the
268 orbital variation or the other forcings due to the nonsignificant correlations. During the
269 period of 5000 BP - 3000 BP, the variation of simulated JJA mean NHT is likely forced
270 by the solar radiation due to the orbital variation (Table 2; the correlation coefficient
271 between the two series is 0.79 at $p < 0.05$), whereas the greenhouse gas change has a
272 comparable negative impact on the JJA mean NHT (the correlation coefficient is -0.73
273 at $p < 0.05$). The melt-water flux also has a moderate contribution to the JJA mean NHT
274 change (the correlation coefficient is 0.48 at $p < 0.05$). For the DJF mean NHT, however,
275 only melt-water flux has a notable negative effect (the correlation coefficient is -0.43 at
276 $p < 0.05$). A two-sided Students t-test is used for the statistical significant test, assuming
277 20 degrees of freedom, which is estimated simply from a 2000-year time series
278 subjected to a 100-year running mean (Delworth and Zeng, 2012). Note that if the
279 effective degree of freedom is used, none of the aforementioned correlation coefficients
280 are significant. The effective degree of freedom is calculated by the following equation:

281

$$N_{dof} = N \times \frac{1 - r_1 \times r_2}{1 + r_1 \times r_2}$$



282 where N_{dof} is the effective degree of freedom regarding to the two correlation samples,
283 N is the total sample size, r_1 and r_2 are autocorrelation lag-1 values for sample 1 and
284 sample 2, respectively (Bretherton et al., 1999).

285 On the other hand, the annual mean NHT difference between the TraCE-ALL run
286 and the sum of the 4 single-forcing sensitivity experiments shows variation similar to
287 the NHT derived from the TraCE-ALL run from 5000 BP to 3000 BP (Fig. S3). The
288 correlation coefficient between these two time-series is 0.66, which is significant above
289 the 95% confidence level (assuming 20 degrees of freedom). We define the difference
290 between the TraCE-ALL run and the sum of the 4 single forcing runs to be the internal
291 variation. Therefore, the internal variation might play a dominant role in the climatic
292 variation during the period of 5000 BP-3000 BP.

293 Moreover, there is no double-peak cooling event during the period of 4400 BP-
294 4000 BP in any single forcing run (Fig. 1, colored lines), which indicates that the 4.2
295 ka BP event might not be triggered by those external forcings, including the orbital, the
296 melt-water flux, the ice-sheets and the greenhouse gases. Volcanic eruptions have been
297 identified as one of the important drivers of climate variation, whereas there were few
298 eruptions during 4400 BP-4000 BP (Sigl et al., 2018). Therefore, we conclude that the
299 4.2 ka BP event is driven by the internal variability. Klus et al. (2017) also suggested
300 that the internal climate variability could trigger abrupt cold events in the North Atlantic
301 without external forcings (e.g., solar irradiance or volcanic).

302 However, why such large variation due to the internal variability occurs at
303 approximately 4.2 ka BP remains unknown. There is little ice-sheet change and no melt
304 water discharge after 5.0 ka BP in the TraCE-ICE run and TraCE-MWF run, and the
305 variations of climate derived from these two runs can thus be considered as internal
306 variabilities. The multicentennial cooling events can also be found in the standardized
307 NHT during the last 5000 years of the two experiments (Fig. S4), and there are drought
308 events in the standardized NH precipitation time series (not shown). However, the
309 timing of those cooling and drought events occurs stochastically. This indicates a
310 general concept of the random variation of the internal mode of the climate system.

311



312 4.2 The mechanisms of the centennial-millennial cooling and drought

313 As has mentioned in Sec. 3.3, the low level NAO-like pattern and upper level
314 CGT-like pattern are the direct mechanisms that cause cooling and megadroughts over
315 most part of the NH. Moreover, the first leading mode of the Empirical Orthogonal
316 Function (EOF) of the annual mean SLP during 5 ka BP-3 ka BP shows a double-peak
317 positive NAO-like pattern but on a centennial scale during the period of 4400 BP-4000
318 BP (Fig. 6). The first leading EOF of geopotential height at 200 hPa after application
319 of a 31-year running mean shows a CGT-like pattern and similar double-peak variation
320 during the period of 4400 BP-4000 BP, which is more obvious after applying the 101-
321 year running mean (Fig. 7). This means that the double-peak cooling and drought of the
322 4.2 ka BP event could be strongly related to the double peak positive NAO-like pattern
323 (at low level) and CGT-like pattern (at high level) at a centennial time scale.

324 Li et al. (2013) suggested that the NAO is a predictor of NHT multidecadal
325 variability during the 20th century. In this study, significant correlation is also found
326 between the annual mean NAO index and the annual mean NHT during the period of
327 4400 BP-4000 BP, with the NAO leading by approximately 40 years (Fig. 8). The NAO
328 index is defined by the first leading mode of the EOF of the SLP. The regressed annual
329 mean surface temperature against the NAO index 40 years earlier during 4400 BP and
330 4000 BP shows cooler NH high latitudes and a warmer SH (Fig. S5), especially the
331 cooling over the northern North Atlantic Ocean, Europe, East Asia and North America.

332 The geopotential height at 200 hPa regressed against the SST over the two North
333 Atlantic outstanding regions (Fig. 4) shows a CGT-like pattern after application of a
334 31-year running mean (Fig. 9), which is similar to the conclusion from Lin et al. (2016)
335 that the CGT could be excited by the AMO-related SST anomaly. The regressed 200
336 hPa geopotential height shows a similar pattern after application of a 101-year running
337 mean (not shown). The anticyclones associated with CGT-like pattern over the West
338 Europe, Central Asia and North America can suppress the precipitation and thus lead to
339 megadrought over these regions.

340 Considering the NAO-like pattern, the CGT-like pattern and the AMO-like pattern
341 together, we suggest that the AMO could be playing a “bridge” role to keep the



342 barotropic structure at the centennial scale, which is similar to the synthesis proposed
343 by Li et al. (2013) that the AMO is a “bridge” that links the NAO and NHT at a
344 multidecadal timescale.

345

346 **5 Conclusion**

347 The characteristics of the 4.2 ka BP event along with the potential drivers and the
348 mechanisms are investigated using a set of transient climate simulations. The simulated
349 event is characterized by hemispheric cooling and megadrought over the NH, whereas
350 the SH experiences warming (over mid-latitude ocean) and wet conditions during this
351 event. The annual mean temperature change is dominated by the boreal winter change.
352 The cool and dry NH and warm and wet SH pattern indicates a southward shift of the
353 ITCZ, as suggested by the reconstructions. These characteristics could also be related
354 to a weakening of the AMOC, which needs further investigation.

355 By comparison between the all-forcing experiment and the single-forcing
356 sensitivity experiments, the 4.2 ka BP event can largely be attributed to the internal
357 variability, although the orbital forcing and the greenhouse gases could impact the
358 boreal summer NHT variation. The origin could be in polar regions and the North
359 Atlantic and may influence the NH climate through teleconnections such as the NAO-
360 like pattern and the CGT-like pattern. The positive NAO-like pattern in the atmosphere
361 triggers cooling over the NH and the negative AMO-like pattern in the ocean, which
362 may last for decades or even centuries. The negative AMO-like pattern triggers CGT-
363 like wave patterns at a multidecadal-centennial time scale accompanied by anticyclones
364 over West Europe, Central Asia and North America, which induce megadrought over
365 those regions. The simplified diagram of the mechanism is shown in Fig. 10.

366 Our findings provide a global pattern and mechanical background of the 4.2 ka BP
367 event that can help better understanding this event. We attributed the internal
368 variabilities to be an essential forcing of the 4.2 ka BP event; however, why it occurs at
369 approximately 4400 BP to 4000 BP remains unknown. Why the SST forcing in the
370 North Atlantic can be maintained at a multidecadal-centennial time scale requires more
371 study. Whether or not the external forcings have modulation effects need to be clarified.



372 Current results are mainly based on annual mean precipitation and temperature,
373 whereas the impacts of external forcings may have seasonal dependence; further
374 investigations are required to evaluate these impacts.

375

376



377 **Acknowledgments**

378 We acknowledge Prof. B Wang for the comments helping to clarify and
379 improve the paper. This research was jointly supported by the National Key Research
380 and Development Program of China (Grant No. 2016YFA0600401), the National
381 Basic Research Program (Grant No. 2015CB953804), the National Natural Science
382 Foundation of China (Grant Nos. 41671197, 41420104002 and 41501210), and the
383 Priority Academic Development Program of Jiangsu Higher Education Institutions
384 (PAPD, Grant No. 164320H116).
385

386 **References:**

- 387 Alley, R., and Agustsdottir, A.: The 8k event: cause and consequences of a major Holocene abrupt
388 climate change, *Quaternary Science Reviews*, 24, 1123-1149, [10.1016/j.quascirev.2004.12.004](https://doi.org/10.1016/j.quascirev.2004.12.004),
389 2005.
- 390 An, C.-B., Tang, L., Barton, L., and Chen, F.-H.: Climate change and cultural response around 4000
391 cal yr B.P. in the western part of Chinese Loess Plateau, *Quaternary Research*, 63, 347-352,
392 [10.1016/j.yqres.2005.02.004](https://doi.org/10.1016/j.yqres.2005.02.004), 2005.
- 393 Bond, G., Kromer, B., Beer, J., Muscheler, R., Evans, M. N., Showers, W., Hoffmann, S., Lotti-
394 Bond, R., Hajdas, I., and Bonani, G.: Persistent solar influence on North Atlantic climate during
395 the Holocene, *Science*, 294, 2130, 2001.
- 396 Booth, R. K., Jackson, S. T., Forman, S. L., Kutzbach, J. E., Bettis, I. E. A., Kreig, J., and Wright,
397 D. K.: A severe centennial-scale drought in mid-continental North America 4200 years ago and
398 apparent global linkages, *The Holocene*, 15, 321-328, 2005.
- 399 Bretherton, C. S., Widmann, M., Dymnikov, V. P., Wallace, J. M., and Bladé, I.: The effective
400 number of spatial degrees of freedom of a time-varying field, *J. Climate*, 12(7), 1990-2009,
401 1999.
- 402 Broccoli, A. J., Dahl, K. A., and Stouffer, R. J.: Response of the ITCZ to Northern Hemisphere
403 cooling, *Geophysical Research Letters*, 33, n/a-n/a, [10.1029/2005gl024546](https://doi.org/10.1029/2005gl024546), 2006.
- 404 Brown, N., and Galbraith, E. D.: Hosed vs. unhosed: interruptions of the Atlantic Meridional
405 Overturning Circulation in a global coupled model, with and without freshwater forcing,
406 *Climate of the Past*, 12, 1663-1679, [10.5194/cp-12-1663-2016](https://doi.org/10.5194/cp-12-1663-2016), 2016.
- 407 Cai, Y., Zhang, H., Cheng, H., An, Z., Lawrence Edwards, R., Wang, X., Tan, L., Liang, F., Wang,
408 J., and Kelly, M.: The Holocene Indian monsoon variability over the southern Tibetan Plateau
409 and its teleconnections, *Earth and Planetary Science Letters*, 335-336, 135-144,
410 [10.1016/j.epsl.2012.04.035](https://doi.org/10.1016/j.epsl.2012.04.035), 2012.
- 411 Clark, P. U., Shakun, J. D., Baker, P. A., Bartlein, P. J., Brewer, S., Brook, E., Carlson, A. E., Cheng,
412 H., Kaufman, D. S., Liu, Z., Marchitto, T. M., Mix, A. C., Morrill, C., Otto-Bliesner, B. L.,
413 Pahnke, K., Russell, J. M., Whitlock, C., Adkins, J. F., Blois, J. L., Clark, J., Colman, S. M.,
414 Curry, W. B., Flower, B. P., He, F., Johnson, T. C., Lynch-Stieglitz, J., Markgraf, V., McManus,
415 J., Mitrovica, J. X., Moreno, P. I., and Williams, J. W.: Global climate evolution during the last
416 deglaciation, *Proceedings of the National Academy of Sciences of the United States of America*,
417 109, E1134-1142, [10.1073/pnas.1116619109](https://doi.org/10.1073/pnas.1116619109), 2012.
- 418 Deininger, M., McDermott, F., Mudelsee, M., Werner, M., Frank, N., and Mangini, A.: Coherency
419 of late Holocene European speleothem $\delta^{18}O$ records linked to North Atlantic Ocean circulation,
420 *Climate Dynamics*, 49, 595-618, [10.1007/s00382-016-3360-8](https://doi.org/10.1007/s00382-016-3360-8), 2017.
- 421 Delworth, T. L., and Zeng, F.: Multicentennial variability of the Atlantic meridional overturning
422 circulation and its climatic influence in a 4000 year simulation of the GFDL CM2.1 climate
423 model, *Geophysical Research Letters*, 39, n/a-n/a, [10.1029/2012gl052107](https://doi.org/10.1029/2012gl052107), 2012.
- 424 Ding, Q., and Wang, B.: Circumglobal Teleconnection in the Northern Hemisphere summer, *Journal*
425 *of Climate*, 18, 3483-3505, 2005.
- 426 Finkenbinder, M. S., Abbott, M. B., and Steinman, B. A.: Holocene climate change in
427 Newfoundland reconstructed using oxygen isotope analysis of lake sediment cores, *Global and*
428 *Planetary Change*, 143, 251-261, [10.1016/j.gloplacha.2016.06.014](https://doi.org/10.1016/j.gloplacha.2016.06.014), 2016.
- 429 Fisher, D., Osterberg, E., Dyke, A., Dahl-Jensen, D., Demuth, M., Zdanowicz, C., Bourgeois, J.,



- 430 Koerner, R. M., Mayewski, P., Wake, C., Kreutz, K., Steig, E., Zheng, J., Yalcin, K., Goto-
431 Azuma, K., Luckman, B., and Rupper, S.: The Mt Logan Holocene—late Wisconsinan isotope
432 record: tropical Pacific—Yukon connections, *The Holocene*, 18, 667-677,
433 10.1177/0959683608092236, 2008.
- 434 Fleitmann, D., Burns, S. J., Mangini, A., Mudelsee, M., Kramers, J., Villa, I., Neff, U., Al-Subbary,
435 A. A., Buettner, A., Hippler, D., and Matter, A.: Holocene ITCZ and Indian monsoon dynamics
436 recorded in stalagmites from Oman and Yemen (Socotra), *Quaternary Science Reviews*, 26,
437 170-188, 10.1016/j.quascirev.2006.04.012, 2007.
- 438 He, F., Shakun, J. D., Clark, P. U., Carlson, A. E., Liu, Z., Otto-Bliesner, B. L., and Kutzbach, J. E.:
439 Northern Hemisphere forcing of Southern Hemisphere climate during the last deglaciation,
440 *Nature*, 494, 81-85, 10.1038/nature11822, 2013.
- 441 He, F.: *Simulating Transient Climate Evolution of the Last deglaciation with CCSM3*, Doctor of
442 Philosophy, Atmospheric and Oceanic Sciences, University of Wisconsin-Madison, 161 pp.,
443 2011.
- 444 Huang, C. C., Pang, J., Zha, X., Su, H., and Jia, Y.: Extraordinary floods related to the climatic event
445 at 4200 a BP on the Qishuihe River, middle reaches of the Yellow River, China, *Quaternary
446 Science Reviews*, 30, 460-468, 10.1016/j.quascirev.2010.12.007, 2011.
- 447 Jansen, E., Overpeck, J. T., Briffa, K. R., Duplessy, J.-C., Joos, F., Masson-Delmotte, V., Olago, D.,
448 Otto-Bliesner, B., Peltier, W. R., Rahmstorf, S., Ramesh, R., Raynaud, D., Rind, D. H.,
449 Solomina, O., Villalba, R., and Zhang, D.: *Palaeoclimate*. In: *Climate Change 2007: The
450 Physical Science Basis*. , Cambridge University Press, Cambridge, United Kingdom and New
451 York, NY, USA, 2007.
- 452 Klus, A., Prange, M., Varma, V., Tremblay, L. B., and Schulz, M.: Abrupt cold events in the North
453 Atlantic in a transient Holocene simulation, *Climate of the Past Discussions*, 1-23, 10.5194/cp-
454 2017-106, 2017.
- 455 Lauritzen, S.-E.: Reconstruction of Holocene climate records from speleothems, in: *Global Change
456 in the Holocene*, edited by: Mackay, A., Battarbee, R., Birks, H. J. B., and Oldfield, F., Arnold,
457 London, 242-263, 2003.
- 458 Li, J., Sun, C., and Jin, F.-F.: NAO implicated as a predictor of Northern Hemisphere mean
459 temperature multidecadal variability, *Geophysical Research Letters*, 40, 5497-5502,
460 10.1002/2013gl057877, 2013.
- 461 Lin, J.-S., Wu, B., and Zhou, T.-J.: Is the interdecadal circumglobal teleconnection pattern excited
462 by the Atlantic multidecadal Oscillation?, *Atmospheric and Oceanic Science Letters*, 9, 451-
463 457, 10.1080/16742834.2016.1233800, 2016.
- 464 Liu, Y. H., Sun, X., and Guo, C. Q.: Records of 4.2 ka BP Holocene Event from China and Its Impact
465 on Ancient Civilizations, *Geological Science and Technology Information (in Chinese)*, 32, 99-
466 106, 2013.
- 467 Liu, Z. Y., Otto-Bliesner, B., He, F., Brady, E. C., Tomas, R. A., Clark, P. U., Carlson, A. E., Lynch-
468 Stieglitz, J., Curry, W., Brook, E., Erickson, D. J., Jacob, R., Kutzbach, J., and Cheng, J.:
469 Transient simulation of Last Deglaciation with a new mechanism for Bolling-Allerod Warming,
470 *Science*, 325, 310-314, 2009.
- 471 Liu, Z., Carlson, A. E., He, F., Brady, E. C., Otto-Bliesner, B. L., Briegleb, B. P., Wehrenberg, M.,
472 Clark, P. U., Wu, S., Cheng, J., Zhang, J., Noone, D., and Zhu, J.: Younger Dryas cooling and
473 the Greenland climate response to CO₂, *Proceedings of the National Academy of Sciences of*



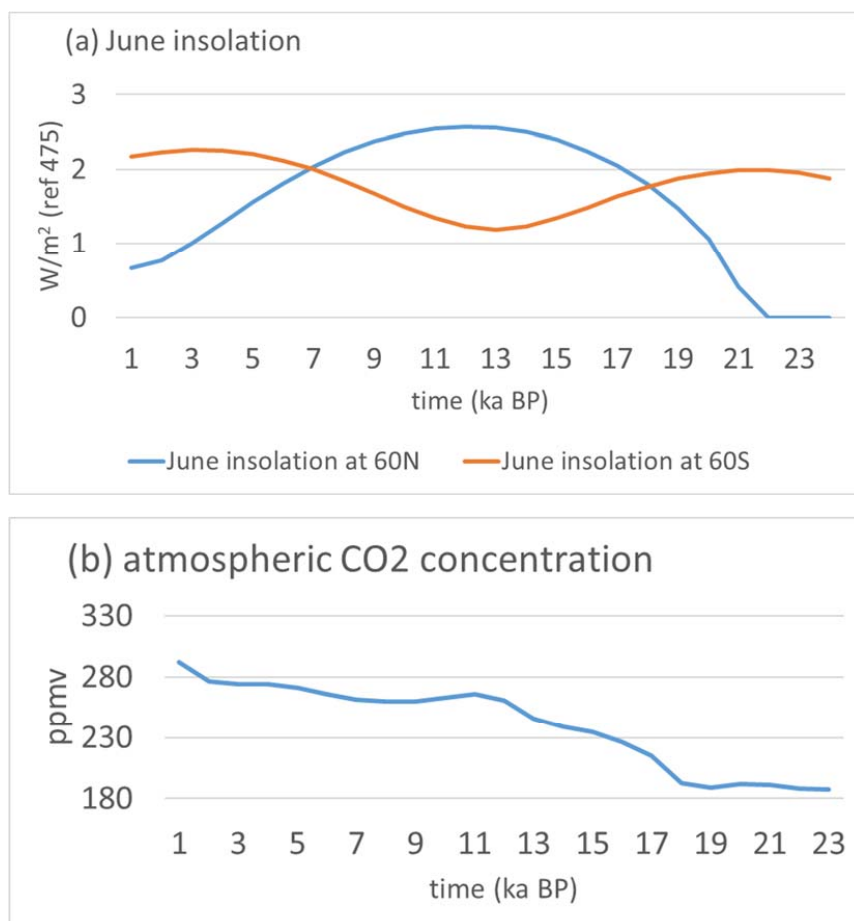
- 474 the United States of America, 109, 11101-11104, 10.1073/pnas.1202183109, 2012.
- 475 Liu, Z., Lu, Z., Wen, X., Otto-Bliesner, B. L., Timmermann, A., and Cobb, K. M.: Evolution and
476 forcing mechanisms of El Niño over the past 21,000 years, *Nature*, 515, 550-553,
477 10.1038/nature13963, 2014.
- 478 Ljung, K., Björck, S., Renssen, H., and Hammarlund, D.: South Atlantic island record reveals a
479 South Atlantic response to the 8.2 kyr event, *Clim. Past*, 4, 35-45, 2008.
- 480 Matero, I. S. O., Gregoire, L. J., Ivanovic, R. F., Tindall, J. C., and Haywood, A. M.: The 8.2 ka
481 cooling event caused by Laurentide ice saddle collapse, *Earth and Planetary Science Letters*,
482 473, 205-214, 10.1016/j.epsl.2017.06.011, 2017.
- 483 Mayewski, P. A., Rohling, E. E., Curt Stager, J., Karlén, W., Maasch, K. A., Meeker, L. D., Meyerson,
484 E. A., Gasse, F., van Kreveld, S., Holmgren, K., Lee-Thorp, J., Rosqvist, G., Rack, F.,
485 Staubwasser, M., Schneider, R. R., and Steig, E. J.: Holocene Climate Variability, *Quaternary
486 Research*, 62, 243-255, 10.1016/j.yqres.2004.07.001, 2004.
- 487 Morrill, C., LeGrande, A. N., Renssen, H., Bakker, P., and Otto-Bliesner, B. L.: Model sensitivity
488 to North Atlantic freshwater forcing at 8.2 ka, *Climate of the Past*, 9, 955-968, 10.5194/cp-9-
489 955-2013, 2013.
- 490 Morrill, C., Ward, E. M., Wagner, A. J., Otto-Bliesner, B. L., and Rosenbloom, N.: Large sensitivity
491 to freshwater forcing location in 8.2 ka simulations, *Paleoceanography*, 29, 930-945,
492 10.1002/2014pa002669, 2014.
- 493 Nakamura, A., Yokoyama, Y., Maemoku, H., Yagi, H., Okamura, M., Matsuoka, H., Miyake, N.,
494 Osada, T., Adhikari, D. P., Dangol, V., Ikehara, M., Miyairi, Y., and Matsuzaki, H.: Weak
495 monsoon event at 4.2 ka recorded in sediment from Lake Rara, Himalayas, *Quaternary
496 International*, 397, 349-359, 10.1016/j.quaint.2015.05.053, 2016.
- 497 Peltier, W. R.: GLOBAL GLACIAL ISOSTASY AND THE SURFACE OF THE ICE-AGE EARTH:
498 The ICE-5G (VM2) Model and GRACE, *Annual Review of Earth and Planetary Sciences*, 32,
499 111-149, 10.1146/annurev.earth.32.082503.144359, 2004.
- 500 Ramos-Román, M. J., Jiménez-Moreno, G., Camuera, J., García-Alix, A., Anderson, R. S., Jiménez-
501 Espejo, F. J., and Carrión, J. S.: Holocene climate aridification trend and human impact
502 interrupted by millennial- and centennial-scale climate fluctuations from a new sedimentary
503 record from Padul (Sierra Nevada, southern Iberian Peninsula), *Climate of the Past*, 14, 117-
504 137, 10.5194/cp-14-117-2018, 2018.
- 505 Rimbu, N., Lohmann, G., Lorenz, S. J., Kim, J. H., and Schneider, R. R.: Holocene climate
506 variability as derived from alkenone sea surface temperature and coupled ocean-atmosphere
507 model experiments, *Climate Dynamics*, 23, 215-227, 10.1007/s00382-004-0435-8, 2004.
- 508 Roland, T. P., Caseldine, C. J., Charman, D. J., Turney, C. S. M., and Amesbury, M. J.: Was there a
509 '4.2 ka event' in Great Britain and Ireland? Evidence from the peatland record, *Quaternary
510 Science Reviews*, 83, 11-27, 10.1016/j.quascirev.2013.10.024, 2014.
- 511 Sachs, J. P.: Cooling of Northwest Atlantic slope waters during the Holocene, *Geophysical Research
512 Letters*, 34, 10.1029/2006gl028495, 2007.
- 513 Shakun, J. D., Clark, P. U., He, F., Marcott, S. A., Mix, A. C., Liu, Z., Otto-Bliesner, B., Schmittner,
514 A., and Bard, E.: Global warming preceded by increasing carbon dioxide concentrations during
515 the last deglaciation, *Nature*, 484, 49-54, 10.1038/nature10915, 2012.
- 516 Shanahan, T. M., Overpeck, J. T., Anchukaitis, K. J., Beck, J. W., Cole, J. E., Dettman, D. L., Peck,
517 J. A., Scholz, C. A., and King, J. W.: Atlantic forcing of persistent drought in West Africa,



- 518 Science, 324, 377-380, 2009.
- 519 Sigl, M., Severi, M., and McConnell, J. R.: A role for volcanoes in causing the "4.2 ka BP event"?,
520 The 4.2 ka BP event: an international workshop, Pisa, Italy, 2018,
- 521 Solomina, O. N., Bradley, R. S., Hodgson, D. A., Ivy-Ochs, S., Jomelli, V., Mackintosh, A. N., Nesje,
522 A., Owen, L. A., Wanner, H., Wiles, G. C., and Young, N. E.: Holocene glacier fluctuations,
523 Quaternary Science Reviews, 111, 9-34, 10.1016/j.quascirev.2014.11.018, 2015.
- 524 Staubwasser, M., and Weiss, H.: Holocene Climate and Cultural Evolution in Late Prehistoric–Early
525 Historic West Asia, Quaternary Research, 66, 372-387, 10.1016/j.yqres.2006.09.001, 2006.
- 526 Staubwasser, M., Sirocko, F., Grootes, P. M., and Segl, M.: Climate change at the 4.2 ka BP
527 termination of the Indus valley civilization and Holocene south Asian monsoon variability,
528 Geophysical Research Letters, 30, 10.1029/2002gl016822, 2003.
- 529 Tan, L. C., An, Z. S., Cai, Y. J., and Long, H.: The Hydrological Exhibition of 4.2 ka BP Event in
530 China and Its Global Linkages, Geological Review (in Chinese), 54, 94-104,
531 10.16509/j.georeview.2008.01.010, 2008.
- 532 Tan, L. C., Cai, Y. J., Cheng, H., Edwards, L. R., Gao, Y. L., Xu, H., Zhang, H. W., and An, Z. S.:
533 Centennial- to decadal- scale monsoon precipitation variations in the upper Hanjiang River
534 region, China over the past 6650 years, Earth and Planetary Science Letters, 360,
535 10.1016/j.epsl.2017.11.044, 2018.
- 536 Tremblay, L. B., Mysak, L. A., and Dyke, A. S.: Evidence from driftwood records for century-to-
537 millennial scale variations of the high latitude atmospheric circulation during the Holocene,
538 Geophysical Research Letters, 24, 2027-2030, 10.1029/97gl02028, 1997.
- 539 Turney, C., Baillie, M., Clemens, S., Brown, D., Palmer, J., Pilcher, J., Reimer, P., and Leuschner,
540 H. H.: Testing solar forcing of pervasive Holocene climate cycles, Journal of Quaternary
541 Science, 20, 511-518, 10.1002/jqs.927, 2005.
- 542 Wagner, A. J., Morrill, C., Otto-Bliesner, B. L., Rosenbloom, N., and Watkins, K. R.: Model support
543 for forcing of the 8.2 ka event by meltwater from the Hudson Bay ice dome, Climate Dynamics,
544 41, 2855-2873, 10.1007/s00382-013-1706-z, 2013.
- 545 Walker, M. J. C., Berkelhammer, M., Björck, S., Cwynar, L. C., Fisher, D. A., Long, A. J., Lowe, J.
546 J., Newnham, R. M., Rasmussen, S. O., and Weiss, H.: Formal subdivision of the Holocene
547 Series/Epoch: a Discussion Paper by a Working Group of INTIMATE (Integration of ice-core,
548 marine and terrestrial records) and the Subcommittee on Quaternary Stratigraphy
549 (International Commission on Stratigraphy), Journal of Quaternary Science, 27, 649-659,
550 10.1002/jqs.2565, 2012.
- 551 Wang, S. W.: 4.2ka BP Event, Advances in Climate Change Research (in Chinese), 6, 75-76, 2010.
- 552 Wang, S. W.: Holocene cold events in the North Atlantic: Chronology and Climate Impact,
553 Quaternary Sciences (in Chinese), 29, 1146-1153, 2009.
- 554 Wanner, H., Beer, J., Bütikofer, J., Crowley, T. J., Cubasch, U., Flückiger, J., Goosse, H., Grosjean,
555 M., Joos, F., Kaplan, J. O., Küttel, M., Müller, S. A., Prentice, I. C., Solomina, O., Stocker, T.
556 F., Tarasov, P., Wagner, M., and Widmann, M.: Mid- to Late Holocene climate change: an
557 overview, Quaternary Science Reviews, 27, 1791-1828, 10.1016/j.quascirev.2008.06.013,
558 2008.
- 559 Weiss, H., and Bradley, R. S.: What drives societal collapse?, Science, 291, 609-610, 2001.
- 560 Weiss, H., Courty, M. A., Wetterstrom, W., Guichard, F., Senior, L., Meadow, R., and Curnow, A.:
561 The Genesis and Collapse of Third Millennium North Mesopotamian Civilization, Science,



- 562 261, 995-1004, 10.1126/science.261.5124.995, 1993.
- 563 Weiss, H.: Global megadrought, societal collapse and resilience at 4.2-3.9 ka BP across the
564 Mediterranean and west Asia, *Past Global Change Magazine*, 24, 62-63,
565 10.22498/pages.24.2.62, 2016.
- 566 Weiss, H.: Megadrought, Collapse, and Resilience in late 3rd millennium BC Mesopotamia, 7th
567 Archaeological Conference of Central Germany, Halle (Saale), 2015.
- 568 Wu, W. X., and Liu T. S.: 4000aB.P. Event and its implications for the origin of Ancient Chinese
569 Civilization, *Quaternary Sciences (in Chinese)*, 21, 443-451, 2001.
- 570 Wu, W. X., and Liu, T. S.: Possible role of the “Holocene Event 3” on the collapse of Neolithic
571 Cultures around the Central Plain of China, *Quaternary International*, 117, 153-166,
572 10.1016/s1040-6182(03)00125-3, 2004.
- 573 Yang, X. P., Scuder, L. A., Wang, X. L., Scuder, L. J., Zhang, D. G., Li, H. W., and al, e.:
574 Groundwater sapping as the cause of irreversible desertification of Hunshandake Sandy Lands,
575 Inner Mongolia, northern China, *PNAS*, 112, 702-706, 2015.
- 576 Zhang, R., and Delworth, T. L.: Impact of Atlantic multidecadal oscillations on India/Sahel rainfall
577 and Atlantic hurricanes, *Geophysical Research Letters*, 33, 10.1029/2006gl026267, 2006.
- 578
- 579



580

581

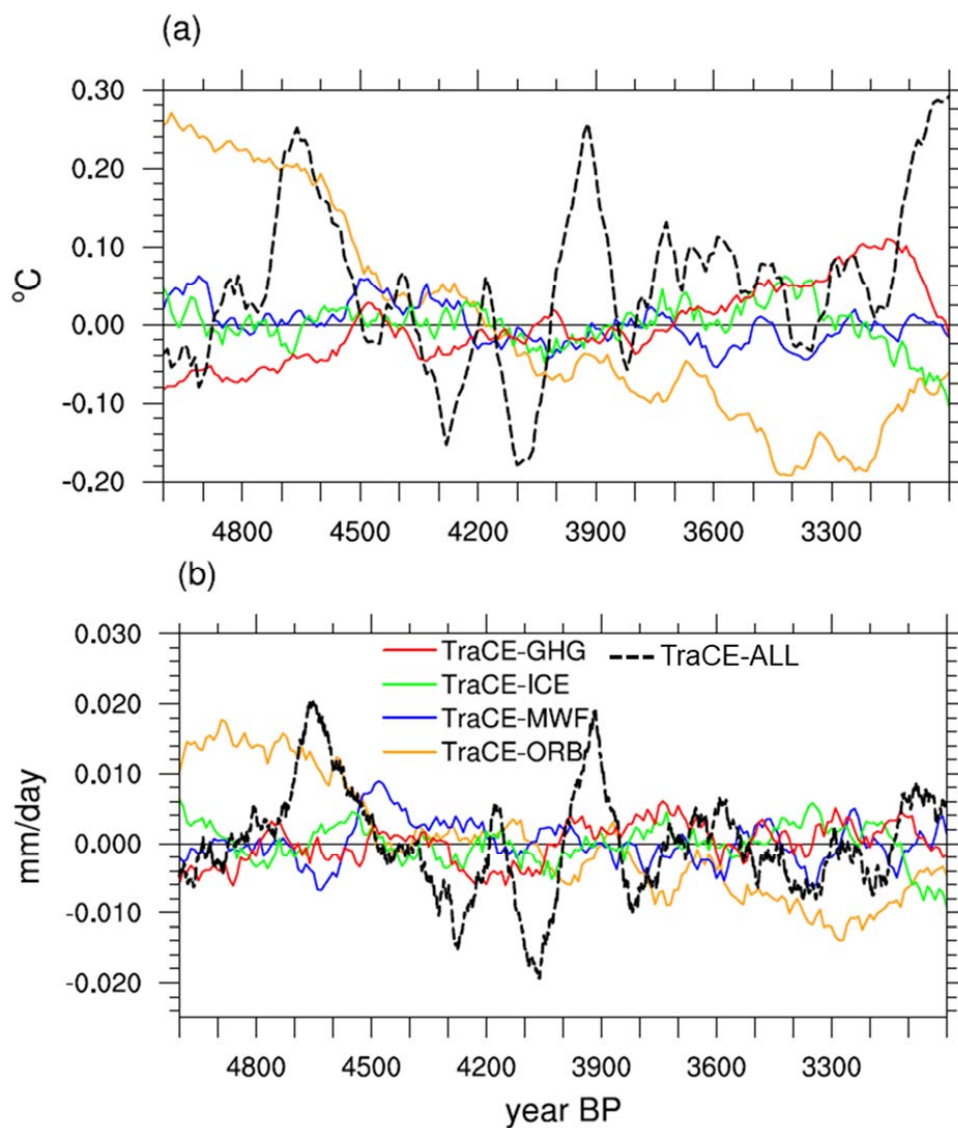
582

583 **Figure 1** Time series of (a) transient June insolation (at 60°N and 60°S) changes
584 resulted from the orbital variation and (b) the transient CO₂ change used in the
585 simulations.

586

587

588



589

590 **Figure 2** Time series of annual mean NH (a) surface temperature anomalies and (b)

591 precipitation anomalies derived from the TraCE-ALL run (dashed black lines) and

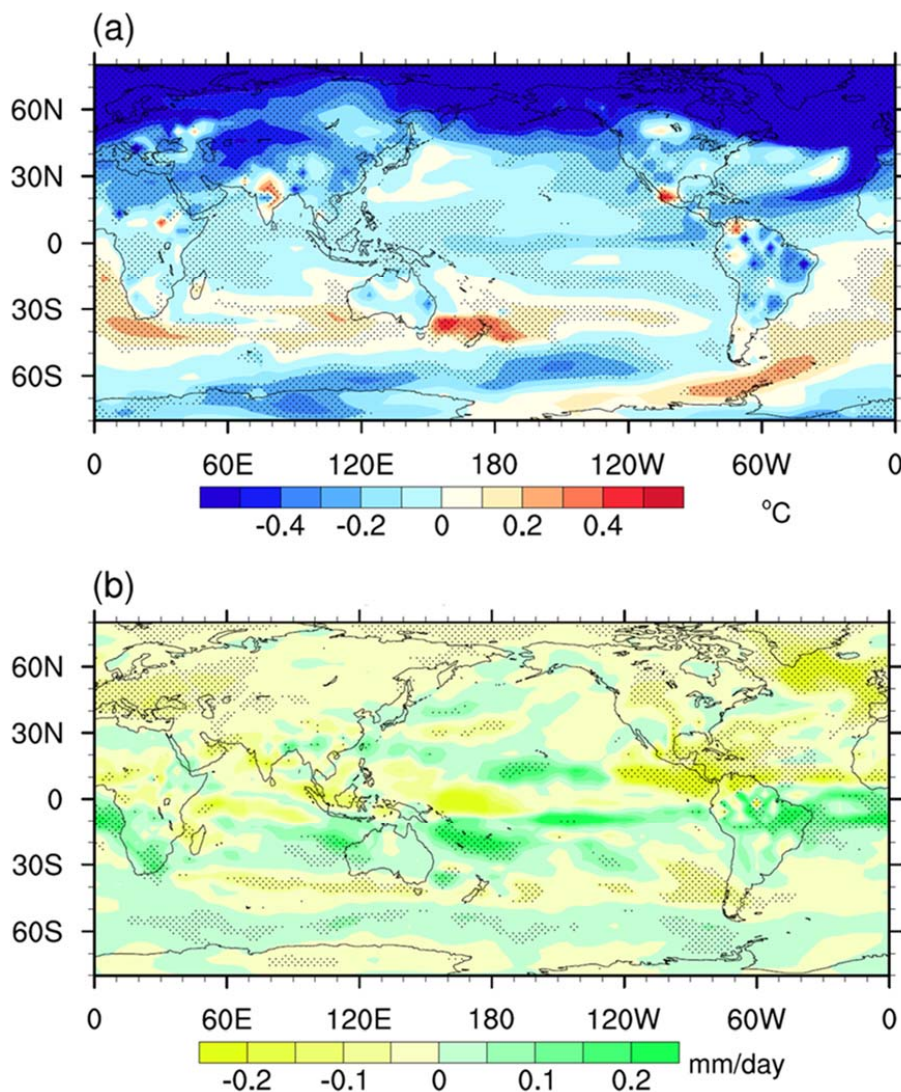
592 each single forcing runs (solid color lines) from 5 ka BP to 3 ka BP. A 101-year

593 running mean has been applied to the time series.

594

595

596



597

598 **Figure 3** Spatial distribution of the annual mean (a) surface temperature and (b)
599 precipitation differences between the cold periods and warm periods. Those regions
600 where significant above 95% confidence level are dotted.

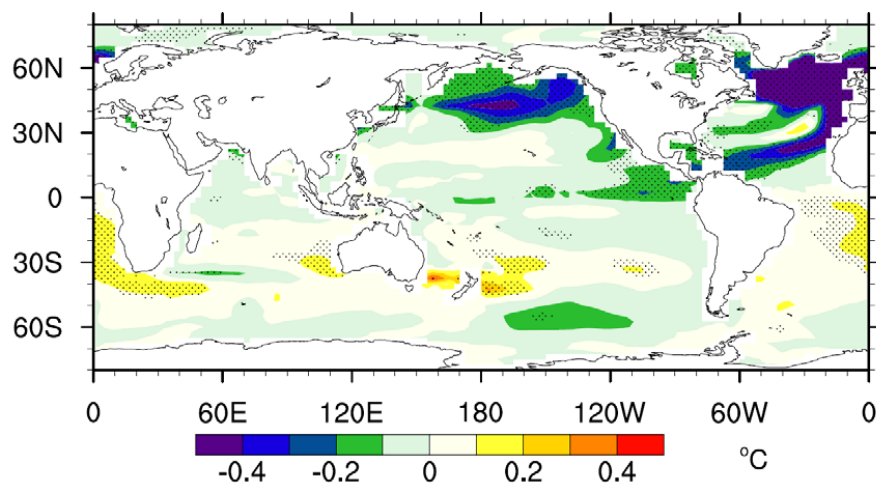
601

602

603



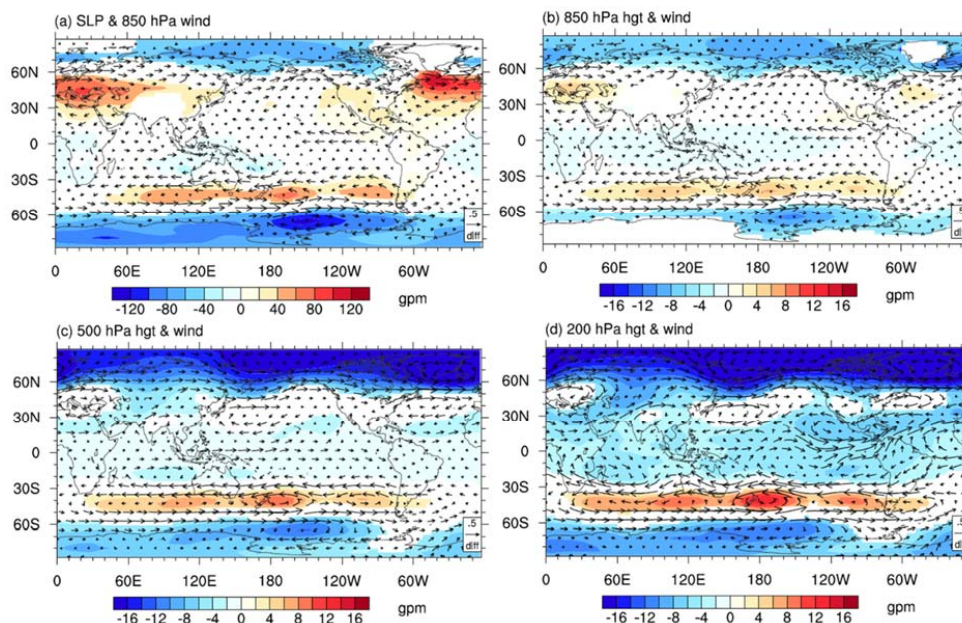
604



605

606 **Figure 4** Spatial distribution of annual mean SST difference between the cold and
607 warm periods. Those regions where significant above 95% confidence level are
608 dotted.
609
610

611



612

613 **Figure 5** Differences of annual mean (a) sea level pressure and 850 hPa wind, (b)
614 geopotential height and wind on 850 hPa, (c) geopotential height and wind on 500
615 hPa and (d) geopotential height and wind on 200 hPa between cold and warm periods.
616 Those regions where significant above 95% confidence level are plotted.

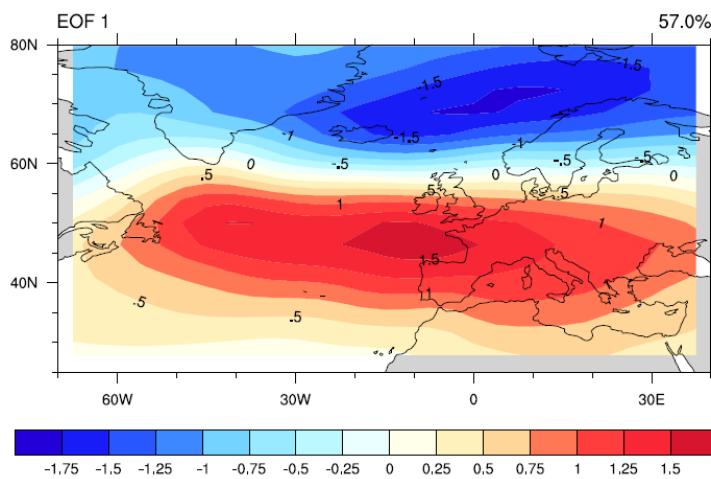
617

618

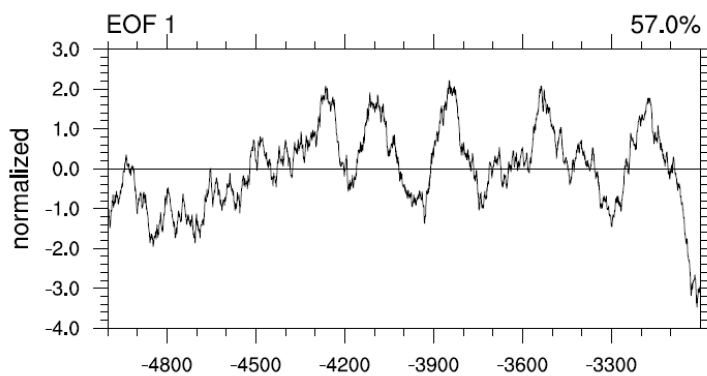
619



620
621



622

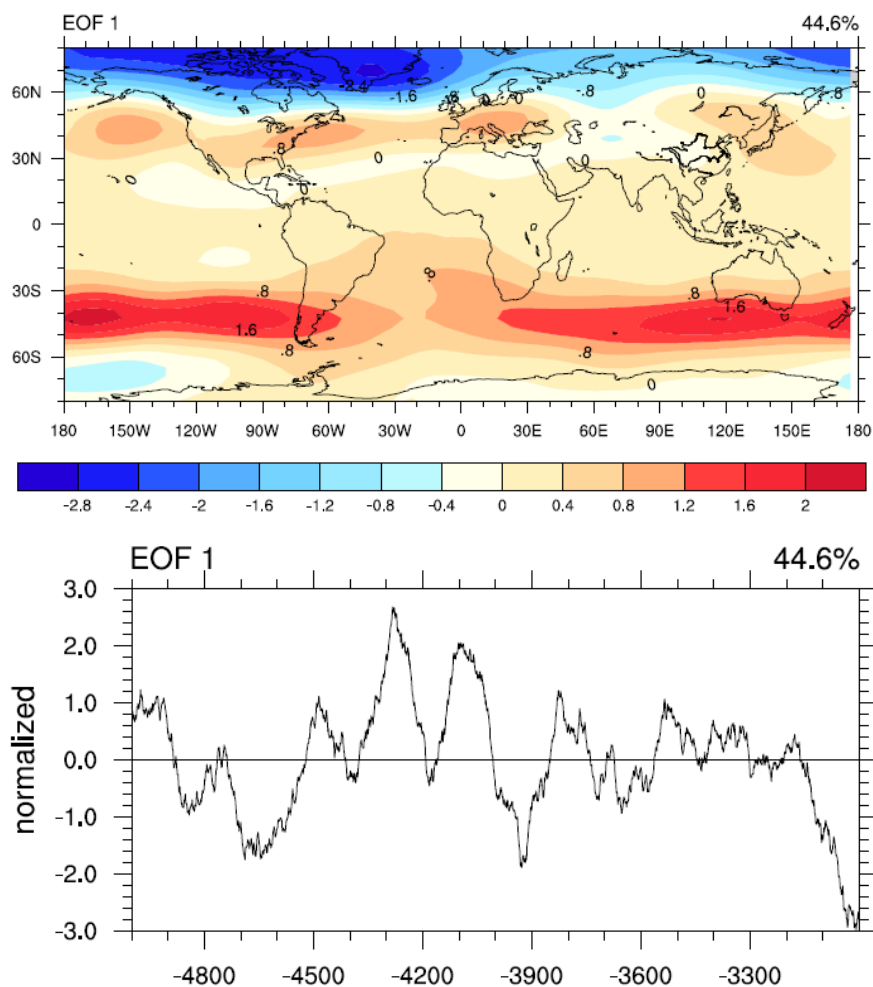


623

624 **Figure 6** Standardized first leading mode of the EOF of annual mean SLP during the
625 period of 5.0 ka BP to 3.0 ka BP after application of a 101-year running mean. The
626 spatial distribution is shown in the top panel, and the time series is shown in the
627 bottom panel. Only this mode passed the North test for EOF.

628
629
630
631
632

633
634



635

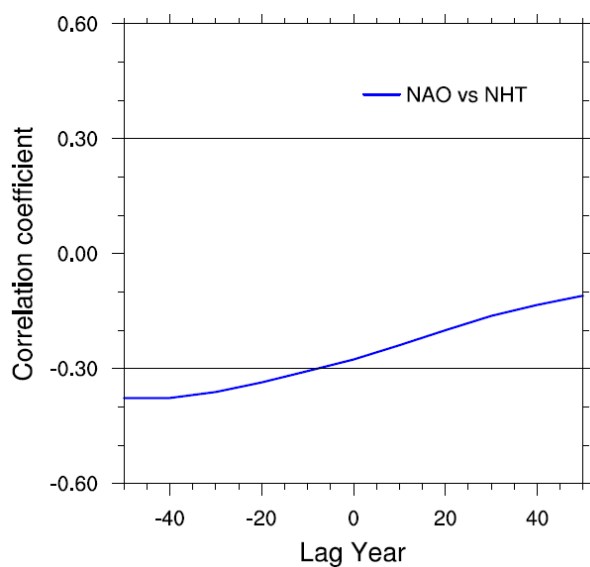
636

637 **Figure 7** Standardized first leading mode of the EOF of annual mean geopotential
638 height at 200 hPa during the period of 5.0 ka BP to 3.0 ka BP after application of a
639 101-year running mean. The spatial distribution is shown in the top panel, and the
640 time series is shown in the bottom panel. Only this mode passed the North test for
641 EOF.

642



643



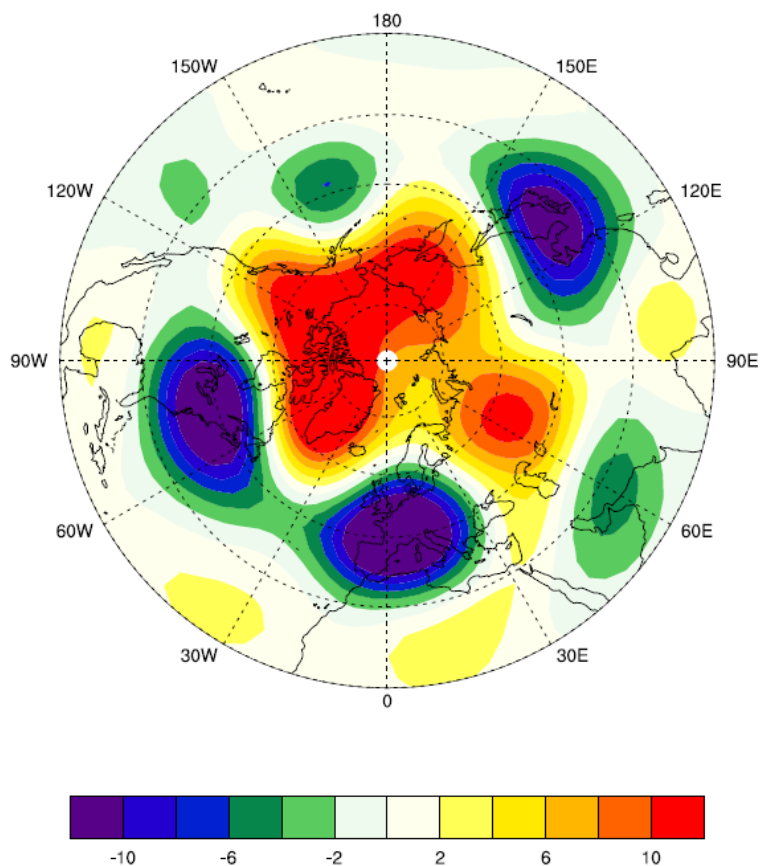
644

645 **Figure 8** Lead-lag correlation between the annual mean North Atlantic Oscillation
646 (NAO) and the North Hemisphere Surface Temperature (NHT) during 4.4 ka BP-4.0
647 ka BP. The black lines (± 0.3) show the significance levels ($p < 0.05$).

648

649

650



651

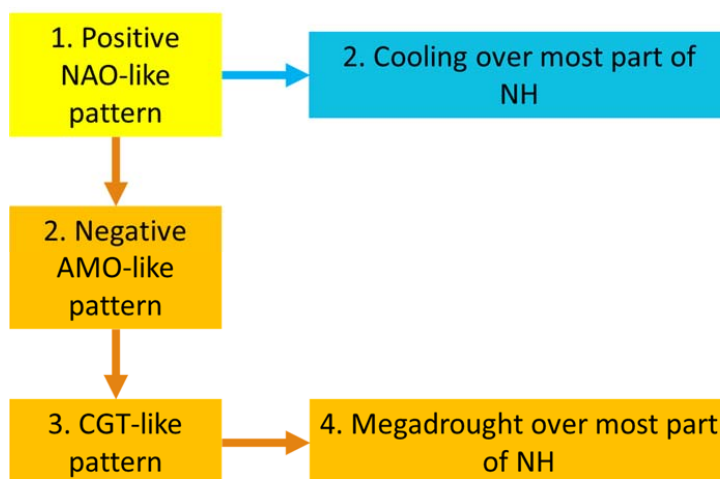
652 **Figure 9** Annual mean geopotential height regressed against the SST over the North

653 Atlantic during 5.0 ka BP - 3.0 ka BP after 31-year running mean application.

654

655

656



657

658 **Figure 10** Schematic diagram shown the mechanisms behind the 4.2 ka BP event.

659

660



661

662 **Table 1** The information of the experiments used in this study.

Experiments	Forcings	Time spanning	Temporal resolution
TraCE-ALL	Orbital, melt-water flux, continental ice-sheet, and Greenhouse gases	22000 BP to 1990 CE	Monthly mean
TraCE-ORB	Orbital only	22000 BP to 1990 CE	Decadal mean
TraCE-MWF	Melt-water flux only	19000 BP to 1990 CE	Decadal mean
TraCE-ICE	Continental ice-sheets only	19000 BP to 1990 CE	Decadal mean
TraCE-GHG	Greenhouse gases only	22000 BP to 1990 CE	Decadal mean

663

664

665

666



667

668

669 **Table 2** Correlation coefficients between the annual mean and seasonal mean NHTs

670 derived from the TraCE-ALL run and those from each single-forcing run from 5.0 ka

671 BP to 3.0 ka BP.

Single forcing run	Annual mean	JJA mean	DJF mean
TraCE-ORB	-0.05	0.79	-0.12
TraCE-MWF	-0.18	0.48	-0.43
TraCE-ICE	-0.30	-0.20	-0.18
TraCE-GHG	0.14	-0.73	0.40

672

673